Supporting Information

# Atomic-scale Spectroscopy of Gated Monolayer $MoS_2$

Xiaodong Zhou[1], Kibum Kang[2], Saien Xie[2], Ali Dadgar[1], Nicholas R. Monahan[3], X.-Y. Zhu[3], Jiwoong Park[2], and Abhay N. Pasupathy[1,†]

[1]*Department of Physics, Columbia University, New York, New York 10027, United States*

[2]*Department of Chemistry and Chemical Biology, Cornell University, Ithaca, New York 14853, United States*

[3]*Department of Chemistry, Columbia University, New York, New York 10027, United States*

## S1. Step edge from monolayer to bilayer $MoS_2$

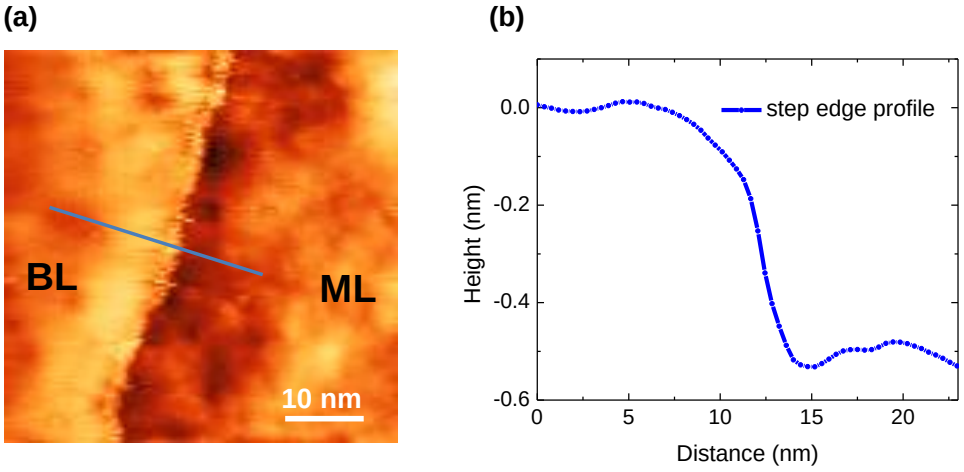


Figure S1. (a) STM topography of a step edge between monolayer (ML) and bilayer (BL) $MoS_2$. (b) A line-cut height profile of the step edge.

We occasionally find bilayer $MoS_2$ patches on our $MoS_2$ films. Figure S1a shows a STM topography of the step edge from monolayer to bilayer $MoS_2$. The apparent step

edge height extracted from this measurement (Figure S1b) is 5 Å, slightly less than the actual single-layer thickness of $MoS_2$ as 6.5 Å. In addition, the bilayer region in the image displays a much smaller height variation than the monolayer region, corroborating our observations in the main text.

## S2. Model calculation of tip-induced band bending (TIBB)

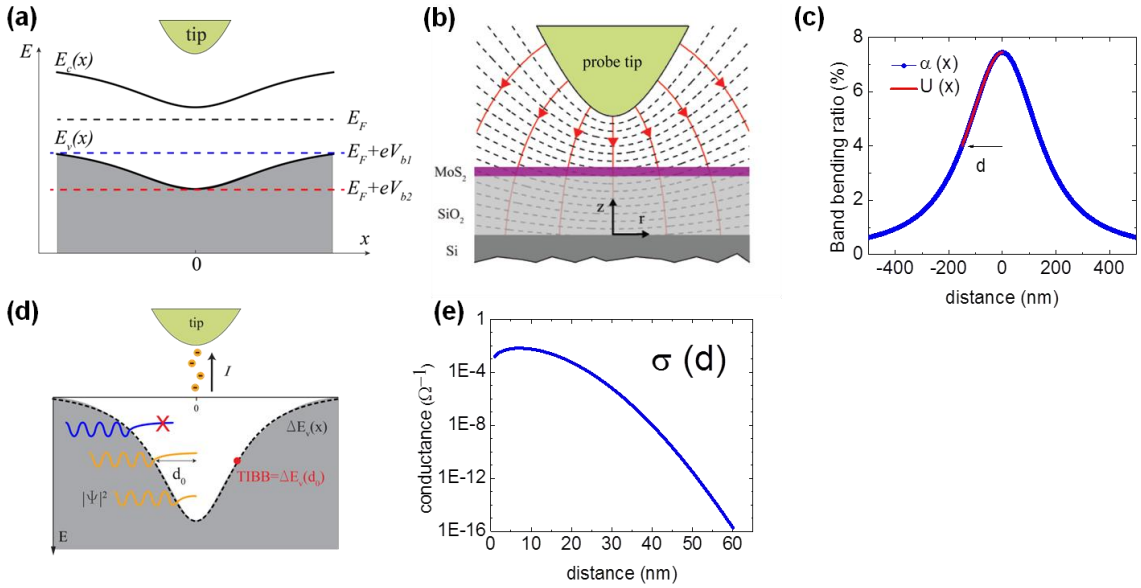


Figure S2. Tip-induced band bending (TIBB) calculations. (a) A band diagram showing TIBB when the tip is positively biased relative to the sample. (b) Schematic of the electrostatic potential distribution in our model where black dashed lines represent equipotential lines and red arrows represent electric field lines. (c) Calculated TIBB ratio α. (d) A reduction of TIBB due to a lateral tunneling process. The valence band states within a lateral distance $d_0$ are accessible for tunneling, thus reduce the observed value of the band bending. (e) Calculated lateral tunneling conductance σ.

As the scanning tip is brought very close to a semiconducting sample surface (~ 5-8 Å), the electric field generated by the tip can easily penetrate the sample due to the poor screening from the sample. During the STS measurement, a large bias voltage is applied to the tip, which essentially acts as an additional electrostatic gate electrode on the sample. The effect of this electric field is to locally charge the sample and bend the

conduction and valence bands underneath the tip.

In Figure S2a we draw a band diagram where both conduction and valence bands are bent downwards when the tip is positively biased relative to the sample. Here the position of the conduction and valence band edges becomes a function of position: $E_{c,v}(x) = E^0_{c,v} + \Delta E_{c,v}(x)$ where $E^0_{c,v}$ refers to the position of the conduction (valence) band at distances far from the tip, and $\Delta E_{c,v}(x)$ is the local band offset due to the tip bias. In what follows, we set the position of the tip to $x = 0$. Thus, $\Delta E_{c,v}(0)$ is the band bending directly under the tip, and $\Delta E_{c,v}(\infty) = 0$. The reason that TIBB always leads to a larger measured gap than the band gap is now clear: when the tip bias $V_{b1}$ is aligned with $E^0_v$ as marked by the blue dashed line in Figure S2a, tunneling continues to be suppressed due to the absence of available valence band states directly under the tip. Instead, the tip bias has to be raised even further to $V_{b2} = E_v(0) = E^0_v + \Delta E_v(0)$ (marked by the red dashed line in Figure S2a) in order to facilitate tunneling to states directly under the tip.

To calculate TIBB, one needs to accurately model the tip and sample's electrostatics in the presence of a tip bias. In what follows, we make a simple analytical estimate of the electrostatics. We first model the tip apex as a ball of radius $r$ with uniform surface charge density determined by the sample bias $V_b$. We then include the conducting back gate electrode, and solve for the local potential on the $MoS_2$ surface using the method of image charges. We assume that this local potential dopes the $MoS_2$ in the same way that the gate electrode does. Figure S2b plots the potential distribution in our model for the case when the tip is positively biased relative to the sample. In cylindrical coordinates, the electric field $E(r, z)$ due to the tip is a function of both radius $r$ and height $z$. This electric field will induce local charge on $MoS_2$ sheet which is located $z_0$ above the back gate electrode surface. We calculate the induced charge density $\sigma$ using Gauss' law $\sigma(r) = \varepsilon_r \varepsilon_0 E_z(r)|_{z=z_0}$. Given the DOS we've already measured for $MoS_2$, we can calculate the TIBB $\Delta\mu(r) = \frac{|\sigma(r)|}{e \cdot DOS}$. In practice, the magnitude of the TIBB is proportional to the applied sample bias $V_b$, so it is useful to define a TIBB ratio $\alpha(r) = \frac{\Delta\mu(r)}{V_b}$. In Figure S2c, we plot the calculated TIBB ratio $\alpha$ assuming a tip radius $r = 50nm$. Right under the tip, it shows the largest TIBB of 7.5% of the applied potential, with a full width

at half maximum of around 300nm.

We now consider the effects of the TIBB on our measured STS spectra. As mentioned before, the bias voltage required to tunnel will be determined by the TIBB directly under the tip, ie, tunneling into the conduction (valence) band directly below the tip will occur when $V_b = E_{c,v}(0) = E_{c,v}^0 + \Delta E_{c,v}(0)$. However, additional tunneling paths exist that allow for tunneling at lower energies. Consider for example a lateral tunneling path such as the one illustrated in Figure S2d. Here, the bias applied to the tip is above $E_v^0$ but below $E_v^0 + \Delta E_v(0)$. In this situation it is energetically impossible to tunnel into valence band states that are directly under the tip. However, it might be possible to tunnel into a valence band state that is located a lateral distance $d$ from the tip, provided that the amplitude of the state is sufficiently large below the tip. In general states located some lateral distance away from the tip will have exponential tails that reach the location directly under the tip and are thus accessible for tunneling (orange waves in Figure S2d). As a simple rule of thumb, if the lateral tunneling conductance between the point under the tip and the valence band states at a distance $d_0$ from the tip is larger than the tip-sample conductance, such paths will contribute to the overall tunneling current. We calculate $d_0$ using the WKB approximation - the lateral tunneling conductance for a hole injected at $x = 0$ at energy $\approx E_v^0 + \Delta E_v(d)$ is given by:

$$\sigma(d) = \frac{2e^2}{h} T = \frac{2e^2}{h} \cdot \frac{2\pi d}{a_0} \cdot exp\left[-2\int_0^d \sqrt{\frac{2m}{\hbar^2} U(x)}\, dx\right]$$

Here $a_0$ is the lattice constant of $MoS_2$ and $U(x)$ is the effective tunnel barrier for an electron at distance x from the center (marked by the red curve in Figure S2c). Using the TIBB $\Delta E_v(x)$ profile previously calculated, we can calculate $\sigma(d)$ as a function of $d$ as shown in Figure S2e which shows an approximately exponentially drop as a function of $d$ as expected. We can compare this in-plane tunneling conductance with the typical STS differential conductance at the edge of the gap $\frac{dI}{dV}(V = E_v)$, which is approximately 1 pS. The condition $\sigma(d_0) \approx \frac{dI}{dV}(V = E_v)$ gives us the approximate lateral range $d_0$ that the tunneling electron sees at a given tunneling bias. From Figure S2e, we see that at the valence band edge, the tunneling electron can tunnel into states that are up to 50 nm away

from the sample. Thus, the effective band bending seen in the tunneling gap is not the value of the band bending directly below the tip $\Delta E_v(0)$ but is instead equal to the band bending at distance $d_0$, ie, $\Delta E_v(d_0)$. Therefore, the tunnel gap exceeds the band gap by the amount $\Delta V_b = \Delta E_c(d_0) + \Delta E_v(d_0)$, which is 140 meV in our case.

**S3. Image potential calculation**

The image potential effect on the band gap of a semiconductor has been extensively studied before. In this effect, the tunneling of electrons into a semiconductor is facilitated by the image force, so the effective energy required for an electron to tunnel is reduced and the band gap is underestimated by an amount equal to the screened exchange difference between conduction and valence bands, that is twice the classical image potential. One can calculate this effect using a classical image potential model: $\Delta E_i = \frac{q^2}{2\pi\varepsilon_0(2d)}$ where d can be taken as the thickness of monolayer $MoS_2$ and $q$ is the screened charge $q = e/_{\varepsilon_r}$. Given $d$~6.5 Å and $\varepsilon_r$~3.9, we get $\Delta E_i$~ 140 $meV$.

**S4. Model simulation of exciton binding energy**

We use a field method described by Smythe and extended by Sritharan to calculate the potential experienced by an electron at (ρ, z) due to the presence of a hole at (0, $z_0$) (Figure 3a in main text):

$$V(\rho,z) = -\frac{e^2}{4\pi\varepsilon_0\varepsilon_2}\left(I_\psi + I_\theta + I_{\text{source}}\right),$$

$$I_\psi = \frac{(\varepsilon_2-\varepsilon_1)(\varepsilon_2-\varepsilon_3)}{\beta_P}\sum_{n=0}^{\infty}\frac{(\beta_N/\beta_P)^n}{\sqrt{(z-z_0-2c+2nc)^2+\rho^2}} + \frac{(\varepsilon_2-\varepsilon_1)(\varepsilon_2+\varepsilon_3)}{\beta_P}\sum_{n=0}^{\infty}\frac{(\beta_N/\beta_P)^n}{\sqrt{(z-z_0-2a+2nc)^2+\rho^2}},$$

$$I_\theta = \frac{(\varepsilon_2-\varepsilon_1)(\varepsilon_2-\varepsilon_3)}{\beta_P}\sum_{n=0}^{\infty}\frac{(\beta_N/\beta_P)^n}{\sqrt{(z-z_0+2c+2nc)^2+\rho^2}} + \frac{(\varepsilon_2+\varepsilon_1)(\varepsilon_2-\varepsilon_3)}{\beta_P}\sum_{n=0}^{\infty}\frac{(\beta_N/\beta_P)^n}{\sqrt{(z-z_0+2b+2nc)^2+\rho^2}},$$

$$I_{\text{source}} = \frac{1}{\sqrt{(z-z_0)^2\rho^2}},$$

where $\beta_N = (\varepsilon_2-\varepsilon_1)(\varepsilon_2-\varepsilon_3)$ and $\beta_P = (\varepsilon_2+\varepsilon_2)(\varepsilon_2+\varepsilon_3)$. The electron and hole were

fixed at the center of the $MoS_2$ layer ($z = z_0 = 0$), which reduces the problem from three- to two-dimensional. The above potential was incorporated into an effective mass Hamiltonian and solved on a 200 nm by 200 nm plane using the finite element method in COMSOL Mutiphysics version 5.0. The simulation yields binding energies of the lowest exciton (1s) of $E_{ex}$ = 280 meV for a $MoS_2$ monolayer on $SiO_2$ which is in good agreement with the experimentally determined exciton binding energy.